
Article:
Mitchinson, B., Arabzadeh, E., Diamond, M.E. et al. (2008) Spike-timing in primary sensory neurons: a model of somatosensory transduction in the rat. Biological Cybernetics, 98 (3). pp. 185-194. ISSN: 0340-1200

https://doi.org/10.1007/s00422-007-0208-7

A computational spike-timing model of transduction in the rat trigeminal pathway.

revision 4

Suggested running title: Computational model of transduction in rat trigeminal pathway.

Keywords: Model, Whisker, Afferent.

B. Mitchinson[1], E. Arabzadeh[2], M. E. Diamond[2], T. J. Prescott[1].

February 3, 2006

[1]Adaptive Behaviour Research Group, Department of Psychology, The University of Sheffield, Sheffield, UK.

[2]Cognitive Neuroscience Sector, International School for Advanced Studies, Trieste, Italy.

Abstract

In previous work, we constructed a simple electro-mechanical model of transduction in the rat mystacial follicle based on statistics of primary afferent responses to a restricted set of whisker deflection stimuli. Here, we update that model using newly available spike-time response data, implementing a more realistic cell membrane, and demonstrate that this updated model can reproduce responses to richer stimuli, including natural textures and pseudo white noise, at a spike-timing level of detail. No modifications were necessary to the mechanical part of the model, representing the physical components of the follicle-sinus complex, supporting its generality. We conclude that this model, and its continued development, will aid in understanding physiological results from higher (e.g. thalamocortical) systems by accurately characterising the signals on which they operate.

1 Introduction

The rat (amongst other mammals) enjoys an impressively acute tactile sensory modality, the sensors of which include large mobile whiskers on either side of the snout (mystacial macrovibrissae) (Waite 2004). This whisker system is considered a particularly accessible model of sensory systems in general, mainly for its unique discrete anatomical organisation, with each whisker represented as a cellular aggregate in several nuclei at all levels of the neuraxis, but also for the controllability and repeatability of whisker-applied stimuli (Woolsey & Van der Loos 1970, Van der Loos 1976, Ma 1991, Ahissar, Sosnik & Haidarliu 2000, Pinto, Brumberg & Simons 2000, Mehta & Kleinfeld 2004). The peripheral parts of the system are (a) the whiskers themselves, each housed in (b) a specialised hair follicle bearing a few hundred mechanoreceptors, which drive (c) a primary afferent nerve, which projects to (d) the trigeminal sensory complex (5s) in brainstem; here, data undergoes some processing and integration, before being passed on to many other nuclei at all levels of the brain (Waite 2004). A complete and accurate characterisation of the signal transduction performed between (a-c), then, will facilitate study of these other nuclei and their associated sensorimotor loops.

To this end, many studies have measured aspects of transduction in the rat whisker-follicle-afferent subsystem, usually using computer-controlled ramp-and-hold whisker deflection stimuli, and recording sequentially from primary afferent cells (Zucker & Welker 1969, Hahn 1971, Gottschaldt, Iggo & Young 1973, Dykes 1975, Gottschaldt & Vahle-Hinz 1981, Gibson & Welker 1983*a*, Gibson & Welker 1983*b*, Lichtenstein, Carvell & Simons 1990, Shoykhet, Doherty & Simons 2000), whilst one recent study recorded from primary afferents during a 'fictive' (electrically induced) whisking against obstacle protocol (Szwed, Bagdasarian & Ahissar 2003). Whilst much data exists, it is difficult to interpret and inter-relate, especially since recording protocols vary between studies as information and technology improve. It is increasingly considered that system modelling can help in this regard, parsimoniously accounting for the richness of the data, and modelling has been used previously to help marshal data from thalamocortical interactions (Rhodes & Llinás 2005), the whisker system in particular (Kyriazi & Simons 1993), and from other tactile transduction systems (Freeman & Johnson 1982, Slavík & Bell 1995, Bensmaïa 2002). We previously reported the only existing model of mystacial transduction in rat, including simulations of the mechanics of the whisker and follicle components and the stimulus-response characteristics of the mechanoreceptor-afferent assembly (Mitchinson, Gurney, Redgrave, Melhuish, Pipe, Pearson, Gilhespy & Prescott 2004). The same model was shown able to well reproduce the response envelopes of the two main categories of primary afferent (rapidly- and slowly-adapting, RA and SA) during simulated protocols of direct whisker deflection and fictive whisking against obstacles. In the remainder of this section, we briefly review this model as previously presented and new response data that has recently become available. In the remainder of the paper, we go on to test the performance of the existing model using these new data, make modifications to the model as highlighted by deficiencies in that performance, and discuss and interpret these modifications.

FIGURE 1 HERE

FIGURE 2 HERE

The model consists of a mechanical model of the whisker-follicle assembly, and an electrical model of the response of each primary afferent to deformation of mechanoreceptors in the follicle. The mechanical model has components representing the whisker shaft from stimulus contact point to base, and internal components of the follicle including the root and mesenchymal sheaths, the glassy membrane, the ring sinus and the follicle capsule (Rice, Mance & Munger 1986, Ebara, Kumamoto, Matsuura, Mazurkiewicz & Rice 2002), Figure 1. Inputs to the mechanical model are two-dimensional deflections or one-dimensional constraints of the whisker contact point and the follicle capsule (the latter representing drive of the follicle capsule, or whisking), outputs are strains in the 'active' layers (root and mesenchymal sheaths), being the locations of mechanoreceptors presumed to drive the

primary afferents. Thus, diverse stimulation protocols (including all those mentioned above and hopefully new, richer, protocols) can be used to drive the model. We do not modify this part of the model here, see the original work for component parameters and derivation from the biology. The strain from each active layer drives multiple parameterised instantiations of the primary afferent model, which has the form of a noisy integrate-and-fire cell model, preceded by several pre-processing stages implementing measured aspects of cell responses, Figure 2. These stages represent the gain, directional response, non-linearity, saturation, adaptation, and stimulus 'memory' of each individual cell; they are governed by the following equations.

The input is the two-dimensional strain in an active layer, $\mathbf{u}_n = [u_{n,1}, u_{n,2}]$. The gain, β, fixes the cell's response range. The directional response is given by

$$
\begin{aligned}
v_n &= |\mathbf{u}_n| \frac{\sqrt{b^2 - 4c} - b}{2} && (1)\\
b &= -\zeta \cos(\arctan(u_{n,2}/u_{n,1}) - \theta) && (2)\\
c &= (\zeta/2)^2 - (1 - \zeta/2)^2 && (3)
\end{aligned}
$$

This defines a circular function with unity gain at the maximally effective angle (MEA) $\theta \in [0, 2\pi)$, and a gain of $1 - \zeta$ opposite the MEA, $\zeta \in [0, 1]$. The non-linearity is $w_n = v_n^\gamma$, and saturation $x_n = \tanh(w_n)$ caps the cell firing rate. Adaptation to stimulus was modelled as

$$
\begin{aligned}
y_n &= x_n - q_n && (4)\\
q_n &= (1 - \lambda_\mathrm{A}) x_n + \lambda_\mathrm{A} q_{n-1} && (5)\\
\lambda_\mathrm{A} &= \exp(-1/(\tau_\mathrm{A} f_S)) && (6)
\end{aligned}
$$

with $1/f_S$ the sample period of integration and τ_A the adaptation time constant. y_n, thus, closely follows features in x_n with duration much less than τ_A, but responds decreasingly to features with longer durations. Stimulus memory was modelled as

$$
\begin{aligned}
z_n &= \begin{cases} y_n, & y_n > \lambda_\mathrm{M} z_{n-1} \\ \lambda_\mathrm{M} z_{n-1}, & \text{otherwise} \end{cases} && (7)\\
\lambda_\mathrm{M} &= \exp(-1/(\tau_\mathrm{M} f_S)) && (8)
\end{aligned}
$$

where τ_M is the memory time constant. The resulting response-strength, z_n, forms the input of an integrate-and-fire neuronal cell model (Eliasmith & Anderson 2003) which generates the spike train. This consists of a leaky integrator with membrane decay constant $k = 1 - \exp(-1/(\tau_\mathrm{D} f_S))$ that resets when its output reaches a fixed unity threshold (τ_D is the membrane time constant). Gaussian white noise $N(\mu, \sigma^2)$ is added to the injection current, before scaling by the desired maximum firing rate, α. Finally, all spikes are delayed by a fixed time τ_L (not shown) to simulate generation and propagation latency. The parameters of a nominal RA cell from the existing model are given in the first column of Table 1.

TABLE 1 HERE

We wish to broaden the scope of the model: data from any stimulation protocol can feed the model design, and a model with wide scope will better predict ganglion responses to arbitrary stimulation. More specifically, the existing model was designed for reproduction of statistical response profiles, and we wish to reproduce spike-time data to test the hypothesis that first-order neuron responses could be governed by a reasonably simple electro-mechanical model, even at this level of detail. Encouragingly, recent modelling of mechanoreceptor responses in macaque monkey mechanoreceptors (Bensmaïa 2002, Bensmaïa, Sripati & Johnson 2005), expanding on the work of Freeman & Johnson (1982), shows

that good performance can be achieved in reproduction of spike-timing in these mechanoreceptors using a simple integrate-and-fire model that is a special case of the integrate-and-fire model used above, under one-dimensional deformation stimulation. Previously, spike-time data, or response data for more general stimuli, were unavailable for the rat whisker periphery. However, recent work by Arabzadeh, Zorzin & Diamond (2005) has made available primary afferent spike-time data in response to carefully controlled and observed, and richer stimuli. These data indicate that, at least some, primary afferents express no apparent stimulus memory, but do express both absolute and relative refractory behaviour – these aspects of cell behaviour are realistic in theory and easily modelled (Eliasmith & Anderson 2003) and have been used successfully in a previous mechanoreceptor model (Slavík & Bell 1995); these will be the non-parametric modifications introduced to the model herein.

Arabzadeh et al. (2005) used a recording protocol as follows. In one set of urethane-anaesthetised rats, whisking was artificially induced (through electrical stimulation of the facial nerve) whilst six different stimuli were presented to one intact whisker (free-space and five textured surfaces). Meanwhile, the two-dimensional movement of the whisker base (1mm from skin) was recorded using an optical sensor, providing a set of whisker base movements that presumably are within the set that the rat would naturally encounter during normal behaviour. In an independent set of urethane-anaesthetised rats, recordings were made of single primary afferent cells whilst these pre-recorded stimuli were played back to a single whisker stub at 1mm from the skin using a piezo-electric actuator. First, these stimuli were repeated as recorded, with each 'whisk' different. Next, a single stimulus consisting of two free whisks followed by two whisks against a texture was repeated identically multiple times, so that for each application the stimulus was as identical as the actuator would allow. Thereafter, for each cell, a long pseudo-random white Gaussian noise signal was presented at the actuator whilst recording continued. In both cases, signals were band-limited to 500Hz before presentation to the actuator, to accommodate its response limits. We will refer to these two protocols as 'natural' and 'noise', respectively. Note that, in contrast to responses in brainstem and above, responses in primary afferents are not observed to vary with anaesthetic level.

The natural data is the important set to fit, since it has primary afferent cells doing their job – encoding natural stimuli. The noise data, however, is useful for generating and tuning models – in the absence of a parametric model, this type of noise is a good choice of input perturbation for system identification, at least for open-loop systems such as this, and provided the signal is sufficiently long (600 seconds, here) (Godfrey 1993). We therefore hand-tune the model using the noise data and test the result on the natural data. We tune a model to only a single recorded cell; thus, we intend to prove the principle that first-order neuron responses in the rat trigeminal ganglion could be governed by a reasonably simple feed-forward model of the mechano-electric transduction mediated by the whisker-follicle-afferent system. We accept that such a model may not well describe all cells, but presume that appropriate tuning might reproduce the behaviour of others. The cell we choose is that named 'Zurvan' in the original work, since its properties are thoroughly described therein, and its performance was precise and reliable.

2 Methods

We drive the model in a manner analogous to the stimulation protocol used by Arabzadeh et al. (2005). Our simulated stimulation is applied at 1mm from the skin using a 'perfect' actuator. Meanwhile, the follicle capsule is allowed to move (i.e. it is constrained only by the tissues of the mystacial pad).

Four model tuning iterations are performed – as models of Zurvan, these are labelled Z1-Z4. To assess the performance of a model on the noise data, we compare recorded spike trains and those generated by the model, over the 600 seconds that is available. For each iteration, we adjust the

gain of the primary afferent model (β), if possible, so that the model fires about the same number of spikes as were recorded – this is achieved within 10% for all models but Z2. We then compute the normalised histogram of inter-spike-intervals (ISI) of each train and the normalised cross-correlogram (or *conditional rate* function) of the trains for visual comparison (Rieke, Warland, De Ruyter Van Steveninck & Bialek 1999). Also, for each spike in the recorded train we find the time offset to the nearest spike in the model train, and plot the histogram of these offsets as for the cross-correlogram; by analogy with the inter-spike-interval, we label this the inter-train-interval (ITI). This last permits a quantitative measure of similarity: we count model spikes that fall within some time interval Δt of a recorded spike, and divide this count by the larger of the total number of spikes in each train. This metric equals unity for trains that are identical within Δt; we notate it as $S_{\Delta t}$. Retrospectively, we then set the latency τ_{L} to maximise $S_{0.5}$. All histograms use a bin width of 0.1ms. Finally, we also compute the stimulus-response 'forward correlation' measure used in Arabzadeh et al. (2005) – for each of a discrete set of velocities of the stimulus, we compute the probability of a spike occurring in the window 1-2ms after the velocity feature, to construct a response probability profile, analogous to Figure 10C of that work.

FIGURE 3 HERE

We illustrate these metrics for Zurvan itself in Figure 3 – as a result, the ITI is a delta function, and $S_{\Delta t} = 1.0$ for any Δt. The ISI has periodic features (reflecting the periodic features in the autocorrelation function of the Chebyshev-filtered stimulus), and an absolute refractory period of around 1.5ms. The response probability profile shows that Zurvan responds most strongly to deflection velocities at an angle of approximately $3\pi/4$. Furthermore, Zurvan responded not at all during the plateau phase of a synchronising step deflection presented before the noise stimulus, so we can conclude that it is a rapidly-adapting (RA) cell. Thus, our nominal model, Z1, will be an RA cell with parameters as described in Mitchinson et al. (2004), and MEA set to $-\pi/4$ (the apparent MEA with respect to whisker stimulation will be as desired, since the whisker shaft lever flips the sense of the stimulus). We hand-tune this model iteratively to reproduce the output of Zurvan as closely as possible; we then test how it performs on natural data. We do not make any changes to the mechanical model previously reported.

FIGURE 4 HERE

FIGURE 5 HERE

As controls, we generate two benchmark models. First, we add normally-distributed noise with standard deviation 0.5ms to Zurvan spike times; results are shown in Figure 4. The ISI is, as expected, a smeared version of the Zurvan ISI. The cross-correlogram displays a strong central peak at $\Delta t = 0$, adjacent nulls corresponding to the refractory period, and settles at longer offsets to a spike probability corresponding to Zurvan's mean firing rate of 114Hz. The ITI plot is identical to the cross-correlogram for short offsets, then falls off quickly as the offset increases – 68% of spikes of this model fall within 0.5ms of a Zurvan spike (reflecting the proportion of normally distributed samples falling within one standard deviation of the mean), $S_{0.5} = 0.68$. Second, we time-shift Zurvan spikes by 1 second, giving us a spike train with identical statistics to Zurvan, but presumably entirely uncorrelated with the stimulus or Zurvan's response. Analysis of this model is shown in Figure 5. Whilst the ISI matches that for Zurvan, the cross-correlogram shows no relationship between the spike trains, similarity is at $S_{0.5} = 0.12$, and the response profile shows no relationship between the spikes and the stimulus.

3 Results

3.1 Tuning with noise data

FIGURE 6 HERE

Z1 The full parameter set of the unmodified model Z1 is reproduced in Table 1, along with the parameters of all subsequent models. The performance is shown in Figure 6. The ISI histogram is very similar to that of Zurvan with noise, but the broad cross-correlogram and $S_{0.5} = 20\%$ indicates that spike-timing performance is poor. This is expected, since this model was tuned against response profiles only, so whilst the statistics of the response reflected in the ISI were captured, the fine structure of spike-timing was not.

FIGURE 7 HERE

Z2 Presented with the natural dataset, Z1 produces bursts of spikes in response to transient features, and this response characteristic can be traced to the model memory. However, Zurvan produces only single spikes in response to these same features, so we drop the memory function for the next model by setting τ_{M}=0. Furthermore, forward correlation (Figure 6C) and inappropriate responses to opposite-MEA stimuli in the natural data (not shown) reveal that Z1 is less well directionally tuned than Zurvan, so we increase the directional tuning parameter to $\zeta = 1.0$. The performance of this model, Z2, can be seen in Figure 7.

FIGURE 8 HERE

Z3, Z4 The model now clearly displays the periodicity present in the Zurvan ISI, and 35% of model spikes now agree well with those of Zurvan. Furthermore, velocity vectors in the half-plane centred on $-\pi/4$ generate only around one percent of the spikes, (six percent for Zurvan itself). There is, however, a very pronounced peak in the model ISI at a latency of under a millisecond, that is entirely missing in Zurvan; Zurvan cannot fire this fast (or, at least, does not under these conditions). As observed above, there is a marked minimum ISI for Zurvan of around 1.5ms – we thus introduce an absolute refractory period to the model, $\tau_{\mathrm{R}} = 1.5$ms, during which period the membrane dynamics are not computed (model Z3).

The very short ISI peak has now been eliminated, but short ISIs of around 3ms are much too frequent (not shown) – Zurvan produces more 6ms ISIs than 3ms, indicating relative refractory behaviour. We model this by introducing a relative refractory period into the mechanoreceptor model, resetting the 'membrane' to a negative value, V_{R}, instead of to zero after the absolute refractory period. we also limit the mechanoreceptor membrane at the lower end at V_{R}, which improves performance. This relative refractory effect, however, has a strong effect over longer intervals than 3ms, so we drop the membrane time constant to 3ms to reduce the relative refractory duration. This latter change compromises the linearity of the membrane model, so we retune the membrane, raising the value of the constant injection current, μ, until linearity is recovered. The performance of the resulting model, Z4, is shown in Figure 8. The ISI and response probability profile are now good visual matches for those of Zurvan, and the ITI and similarity ($S_{0.5} = 0.57$) show further improvement.

FIGURE 9 HERE

Interestingly, performance is robust to changes in the MEA in the range 0.2π to 0.3π, but sensitive to directional tuning – dropping ζ even to 0.95 hurts performance (not shown) – hinting that the directional sensitivity of Zurvan may be less sharp than that of the model (circular). Figure 9 is a plot of the integral of the response probability profile over radius (normalised) for Zurvan and

Z4, compared with a true circular function. Note that though the directional sensitivity function of the model is circular, we do not expect this measured response to be circular, since it includes the non-linear velocity response profile of the model. We note that the measured response from Zurvan is very close to circular, and that of the model rather tighter, but we do not investigate further here since the potential improvement appears minimal.

FIGURE 10 HERE

FIGURE 11 HERE

3.2 Testing with natural data

To test whether the tuned model behaves appropriately in response to natural stimuli, we present the natural dataset to Z4, both the multiple unique stimuli and the multiple repetitions of a single stimulus. The results are shown in Figures 10 and 11, respectively, which are analogous to the panels A-C of Figures 2 and 8, respectively, from the original work. The results are similar in each case, and correspond closely to the response of Zurvan. Z4 responds with approximately one spike to each of the main velocity features to which Zurvan responds; specifically, with a mean of 0.87 spikes/feature to the different stimuli, and with 0.99 spikes/feature to the identical stimuli set. The standard deviation (SD) of Z4 spike times in response to the identical stimuli is sensitive to the sharpness of the driving feature, but for four of the six features it is 0.1-0.2ms, which is comparable with results in the original work for a different cell ($\sim$0.1ms, data for Zurvan not available). The variability in response time to the multiple stimuli set is comparable to that of Zurvan, reflecting that the main source of variability here is the stimulus itself.

For both sets, there is a small amount of response away from the main features, but it is not very marked. This is in reasonable agreement with results from Zurvan, though Zurvan has a noticeably stronger response to retraction during free whisking. We note, however, that the response of Zurvan to free whisking retraction is unreliable even for the repeated stimulus set, indicating that its absence from Z4 may not indicate encoding failure. Overall, the match between Z4 and Zurvan is visually impressive.

4 Discussion

The RA afferent model previously published (Z1) was based on statistical response profiles, probably obfuscated by convolution with actuator response, or with more complex whisker response than was modelled, and was not a good model of Zurvan at a spike-timing level. However, removing the memory component and implementing a more realistic membrane model with refractory effects resulted in a marked performance improvement. The resulting model, Z4, matches almost two thirds of Zurvan spikes in response to a noise stimulus with an accuracy of 0.5ms or better (better than two-thirds for an accuracy of 1.0ms), as opposed to a control model of uncorrelated spikes with the same statistics (Figure 5) which matches only 12% of spikes to this accuracy. Furthermore, both the firing statistics (indicated by the ISI histogram) and the velocity response profile (polar plot) are good matches for those of the real cell, though the directional tuning of the model seems a little too sharp.

FIGURE 12 HERE

Figure 12A illustrates the ganglion cell 'memory effect' in the population response of 81 SA and RA cells to a ramp-and-hold stimulus from Shoykhet et al. (2000) – the 3ms rise ramp of the stimulus (indicated by solid bar) elicits a 30-40ms response. This response does not represent fairly rapid adaptation in some cells, since individual cells typically exhibit very long or short time constants of

adaptation whilst still displaying this medium term response to the transient stimulus component (Lichtenstein et al. 1990, Kyriazi, Carvell & Simons 1994, Jones, Lee, Trageser, Simons & Keller 2004). This effect required the memory component of the original model, which is illustrated in Figure 12B, under the same experimental protocol as used in the experiment reported in panel A. However, no cell studied by Arabzadeh et al. was found to display memory (personal communication). In light of this, it seems likely that the previously observed transient memory effect is not a characteristic of ganglion cells (or, at least, the majority of them). Removing the memory effect in the model and repeating the simulation of Figure 12B gives results as shown in Figure 12C, with a truncated transient response to stimulus onset and offset.

The apparent memory may instead be attributable to some feature of the delivery of stimulus to the mechanoreceptors, probably mechanical ringing (Robichaud, Del Prete & Grigg 2003). Mechanical ringing has been observed in the type of actuators used for primary afferent studies (Simons 1983) though stimulus pre-filtering has typically been used to reduce or eliminate it. Ringing has also been observed in intact whiskers (Hartmann, Johnson, Towal & Assad 2003, Mehta & Kleinfeld 2004), though we are not aware that it has been assessed in trimmed whiskers. Both types of ringing have appropriate time profiles to cause the observed prolonged responses. Some filter designs can also have similar effects (Robichaud et al. 2003) – the Bessel filter suggested in Simons (1983) does not, but that filter cannot be used with high velocity stimuli, and the filtering used in all other studies is unreported. We modelled ringing in the actuator by pre-filtering the stimulus used in Shoykhet et al. (2000) with a filter based on the ringing data from Simons (1983), and repeated the simulation of Figure 12C using this filtered stimulus to drive the model actuator. The result in Figure 12D shows the effective prolonging of the transient responses. Whilst the periodicity introduced by this ringing model is not apparent in the biological population response (panel A), it is apparent in histograms constructed from multiple trials with single biological cells (Lichtenstein et al. 1990, Kyriazi et al. 1994, Jones et al. 2004, Minnery & Simons 2003).

How 'good' is this model performance in real terms? Unfortunately, we do not have cell response data to multiple presentations of the noise stimulus, but responses to multiple presentations of identical natural data suggest that Zurvan can achieve excellent (approaching 100%) spike-for-spike matching between presentations (for spikes in response to 'features' of the stimulus), with timing jitter standard deviation ∼0.1-0.2ms. This is superior to the match between Zurvan and Z4 as shown by the noise data – finding all the spikes that are 'shared' between Zurvan and Z4 in response to the noise data by choosing only those that fall within 0.5ms of each other, and computing the timing jitter of only these spikes, gives 57% shared spikes with a jitter standard deviation of 0.23ms. However, the response of Z4 to the identical natural data shows it to be comparable in reliability to Zurvan in this context, with average 99% spike-for-spike matching and timing jitter standard deviation in the 0.1-0.2ms range for 4 of 6 features (see Figures 10 and 11 for figures).

Furthermore, we might argue that a real or simulated cell cannot usefully encode information at these very high levels of precision, because the noise introduced by variability between samplings of the stimulus (e.g. sandpaper) swamps the intrinsic timing jitter of the cell (timing variability from Zurvan using non-identical stimuli was nearer 1ms). However, this argument requires an assumption that is unlikely to hold – that noise introduced from variability of whisker motion at Zurvan is uncorrelated with noise introduced due to the same variability at Zurvan's sister cells. This assumption might be tested by recording from multiple ganglion cells simultaneously under a multiple non-identical stimulus battery, and comparing intra- and inter-trial correlations between cell responses. Given the very high stimulus reproducibility that is evident from the very high response reproducibility shown in Arabzadeh et al. (2005), it is probably safe to relax the requirement for simultaneous recording.

In summary, we have shown that this simple electro-mechanical model can reproduce much of the behaviour of a rapidly-adapting primary afferent cell in the trigeminal ganglion in response to deflections of the whisker base. In updating the model to achieve this, we have removed the memory

component and added refractory behaviour. Similar performance at this level of detail has been achieved recently in modelling the response of slowly- and rapidly-adapting mechanoreceptors to deflection of hairless skin on the hands of macaque monkeys (Bensmaïa et al. 2005), using a one-dimensional model that is related to that used here. We are increasingly confident that the response of such primary sensory neurons will remain relatively simple as further work improves the accuracy of models, and that accurately describing this encoding should be prioritised by workers wishing to understand the function of higher centres in sensory pathways and cortical sensory processing.

References

Ahissar, E., Sosnik, R. & Haidarliu, S. (2000), 'Transformation from temporal to rate coding in a somatosensory thalamocortical pathway.', *Nature* **406**, 302–306.

Arabzadeh, E., Zorzin, E. & Diamond, M. (2005), 'Neuronal encoding of texture in the whisker sensory pathway.', *Neuron* .

Bensmaïa, S. (2002), 'A transduction model of the meissner corpuscle.', *Math Biosci* **176**, 203–217.

Bensmaïa, S., Sripati, A. & Johnson, K. (2005), A biophysical model of afferent responses to dynamic stimuli. Society for Neuroscience, Washington DC, Program No. 624.12, (Abstract Viewer and Itinerary Planner CDROM or Online).

Dykes, R. (1975), 'Afferent fibers from mystacial vibrissae of cats and seals.', *J Neurophysiol* **38**, 650–662.

Ebara, S., Kumamoto, K., Matsuura, T., Mazurkiewicz, J. & Rice, F. (2002), 'Similarities and differences in the innervation of mystacial vibrissal follicle-sinus complexes in the rat and cat: A confocal microscopic study.', *J Comp Neurol* **449**, 103–119.

Eliasmith, C. & Anderson, C. (2003), *Neural Engineering.*, MIT Press.

Freeman, A. & Johnson, K. (1982), 'Cutaneous mechanoreceptors in macaque monkey: Temporal discharge patterns evoked by vibration, and a receptor model.', *J Physiol* **323**, 21–41.

Gibson, J. & Welker, W. (1983*a*), 'Quantitative studies of stimulus coding in first-order vibrissa afferents of rats. 1. Receptive field properties and threshold distributions.', *Somatosens Res* **1**, 51–67.

Gibson, J. & Welker, W. (1983*b*), 'Quantitative studies of stimulus coding in first-order vibrissa afferents of rats. 2. Adaptation and coding of stimulus parameters.', *Somatosens Res* **1**, 95–117.

Godfrey, K., ed. (1993), *Perturbation Signals for System Identification.*, Prentice Hall.

Gottschaldt, K., Iggo, A. & Young, D. (1973), 'Functional characteristics of mechanoreceptors in sinus hair follicles of the cat.', *J Physiol* **235**, 287–315.

Gottschaldt, K. & Vahle-Hinz, C. (1981), 'Merkel cell receptors: Structure and transducer function.', *Science* **214**, 183–186.

Hahn, J. (1971), 'Stimulus-response relationships in first-order sensory fibres from cat vibrissae.', *J Physiol* **213**, 215–226.

Hartmann, M., Johnson, N., Towal, R. & Assad, C. (2003), 'Mechanical characteristics of rat vibrissae: Resonant frequencies and damping in isolated whiskers and in the awake behaving animal.', *J Neurosci* **23**, 6510–6519.

Jones, L., Lee, S., Trageser, J., Simons, D. & Keller, A. (2004), 'Precise temporal responses in whisker trigeminal neurons.', *J Neurophysiol* **92**, 665–668.

Kyriazi, H., Carvell, G. & Simons, D. (1994), 'Off response transformations in the whisker/barrel system.', *J Neurophysiol* **72**, 392–401.

Kyriazi, H. & Simons, D. (1993), 'Thalamocortical response transformations in simulated whisker barrels.', *J Neurosci* **13**, 1601–1615.

Lichtenstein, S., Carvell, G. & Simons, D. (1990), 'Responses of rat trigeminal ganglion neurons to movements of vibrissae in different directions.', *Somatosens Mot Res* **7**, 47–65.

Ma, P. (1991), 'The barrelettes–architectonic vibrissal representations in the brainstem trigeminal complex of the mouse. I. Normal structural organization.', *J Comp Neurol* **309**, 161–199.

Mehta, S. & Kleinfeld, D. (2004), 'Frisking the whiskers. Patterned sensory input in the rat vibrissa system.', *Neuron* **41**, 181–184.

Minnery, B. & Simons, D. (2003), 'Response properties of whisker-associated trigeminothalamic neurons in rat nucleus principalis.', *J Neurophysiol* **89**, 40–56.

Mitchinson, B., Gurney, K., Redgrave, P., Melhuish, C., Pipe, A., Pearson, M., Gilhespy, I. & Prescott, T. (2004), 'Empirically inspired simulated electro-mechanical model of the rat mystacial follicle-sinus complex.', *Proc R Soc Lond B Biol Sci* **271**, 2509–2516.

Pinto, D., Brumberg, J. & Simons, D. (2000), 'Circuit dynamics and coding strategies in rodent somatosensory cortex.', *J Neurophysiol* **83**, 1158–1166.

Rhodes, P. & Llinás, R. (2005), 'A model of thalamocortical relay cells.', *J Physiol* **565**, 765–781.

Rice, F., Mance, A. & Munger, B. (1986), 'A comparative light microscopic analysis of the sensory innervation of the mystacial pad. I. Innervation of vibrissal follicle-sinus complexes.', *J Comp Neurol* **252**, 154–174.

Rieke, F., Warland, D., De Ruyter Van Steveninck, R. & Bialek, W. (1999), *Spikes: Exploring the Neural Code.*, MIT Press.

Robichaud, D., Del Prete, Z. & Grigg, P. (2003), 'Stretch sensitivity of cutaneous ra mechanoreceptors in rat hairy skin.', *J Neurophysiol* **90**, 2065–2068.

Shoykhet, M., Doherty, D. & Simons, D. (2000), 'Coding of deflection velocity and amplitude by whisker primary afferent neurons: Implications for higher level processing.', *Somatosens Mot Res* **17**, 171–180.

Simons, D. (1983), 'Multi-whisker stimulation and its effects on vibrissa units in rat sml barrel cortex.', *Brain Research* **276**, 178–182.

Slavík, P. & Bell, J. (1995), 'A mechanoreceptor model for rapidly and slowly adapting afferents subjected to periodic vibratory stimuli.', *Math Biosci* **130**, 1–23.

Szwed, M., Bagdasarian, K. & Ahissar, E. (2003), 'Encoding of vibrissal active touch.', *Neuron* **40**, 621–630.

Van der Loos, H. (1976), 'Barreloids in mouse somatosensory thalamus.', *Neuroscience Letters* **2**, 1–6.

Waite, P. (2004), Trigeminal sensory system., *in* G. Paxinos, ed., 'The Rat Nervous System.', Elsevier, pp. 817–851.

Woolsey, T. & Van der Loos, H. (1970), 'The structural organization of layer iv in the somatosensory region (si) of mouse cerebral cortex. the description of a cortical field composed of discrete cytoarchitectonic units.', *Brain Res* **17**, 205–242.

Zucker, E. & Welker, W. (1969), 'Coding of somatic sensory input by vibrissae neurons in the rat's trigeminal ganglion.', *Brain Res* **12**, 138–156.

5 Acknowledgements

This work was funded by EPSRC Research grant no. GR/S19639/01.

Model	nom.	Z1	Z2	Z3	Z4
τ_{D}(ms)	10	.	.	.	3.0
α	2000	.	.	.	.
μ	0.03	.	.	.	0.15
σ	0.1	.	.	.	.
ζ	0.6	.	1.0	.	.
γ	2	.	.	.	.
τ_{A}(ms)	5.0	.	.	.	.
τ_{M}(ms)	5.0	.	0.0	.	.
τ_{R}(ms)				1.5	.
V_{R}					-0.6
MEA		-$\pi/4$	.	.	.
τ_{L}(ms)	3.0	1.0	1.2	1.1	1.4
β	61.5	30	120	250	120

Table 1: Parameters of the nominal RA cell, and progressive models of Zurvan. Dots indicate that this parameter is unchanged (so look left for its value). Empty indicates that this parameter is not applicable to this model.

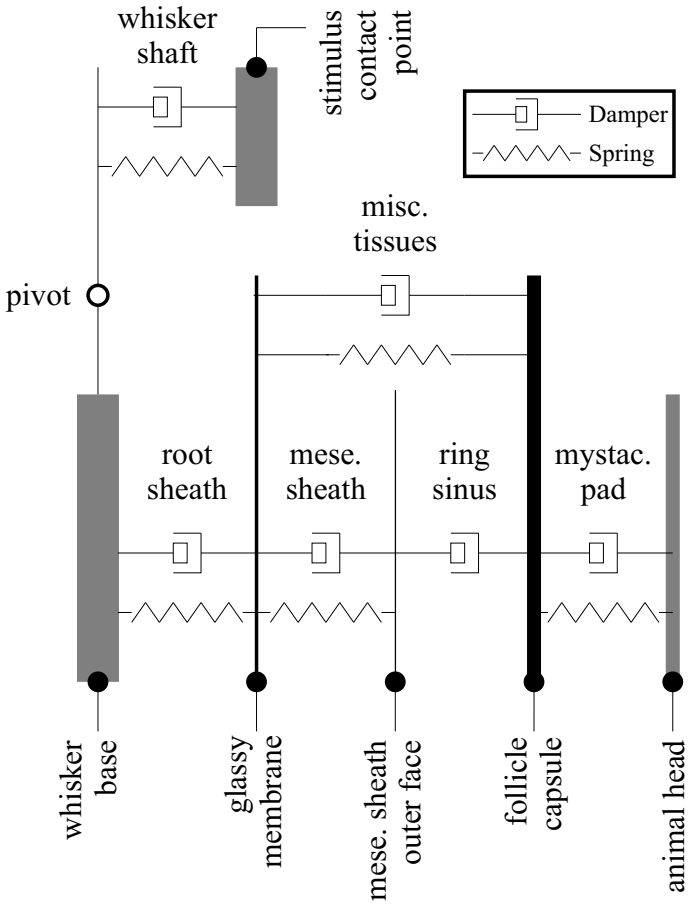

Figure 1: Mechanical part of model. Mass components are represented as blocks, springs and dampers are shown iconically, the pivot of the whisker shaft in the follicle is a circle.

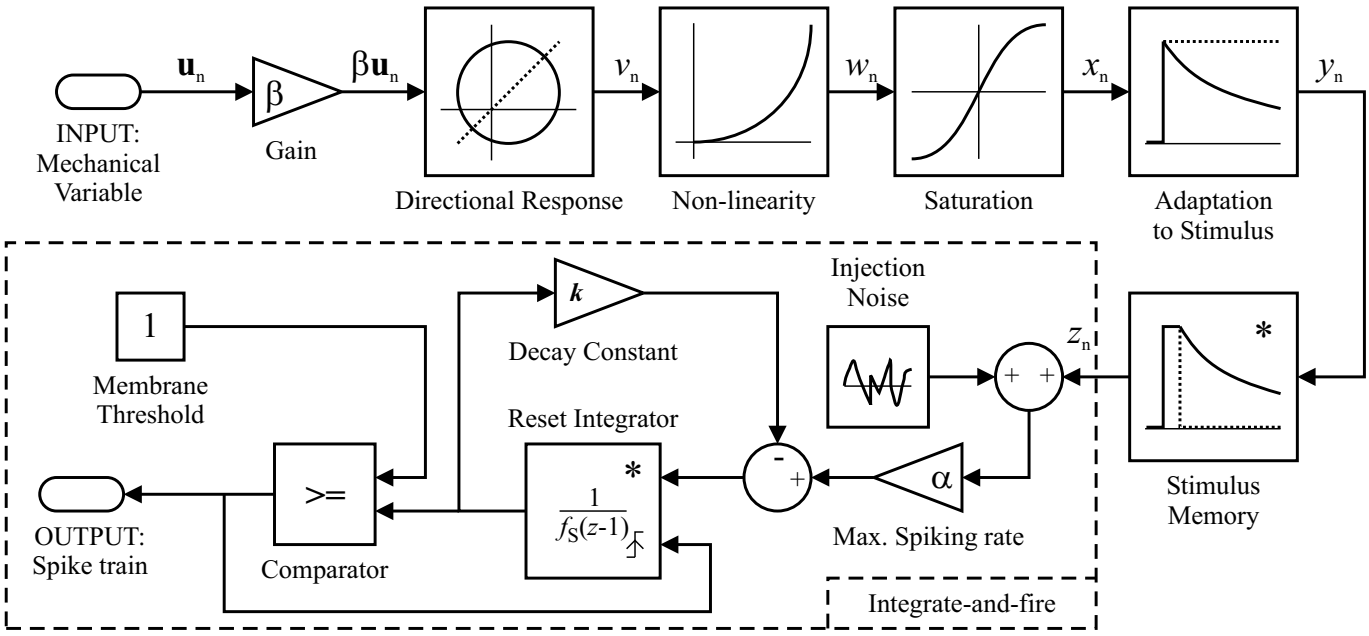

Figure 2: Primary afferent part of model. Pre-processing stages are shown above and to the right, driving a standard noisy integrate-and-fire model enclosed in the dashed region. Items marked with an asterisk (stimulus memory and reset integrator) are modified herein beyond parameter changes.

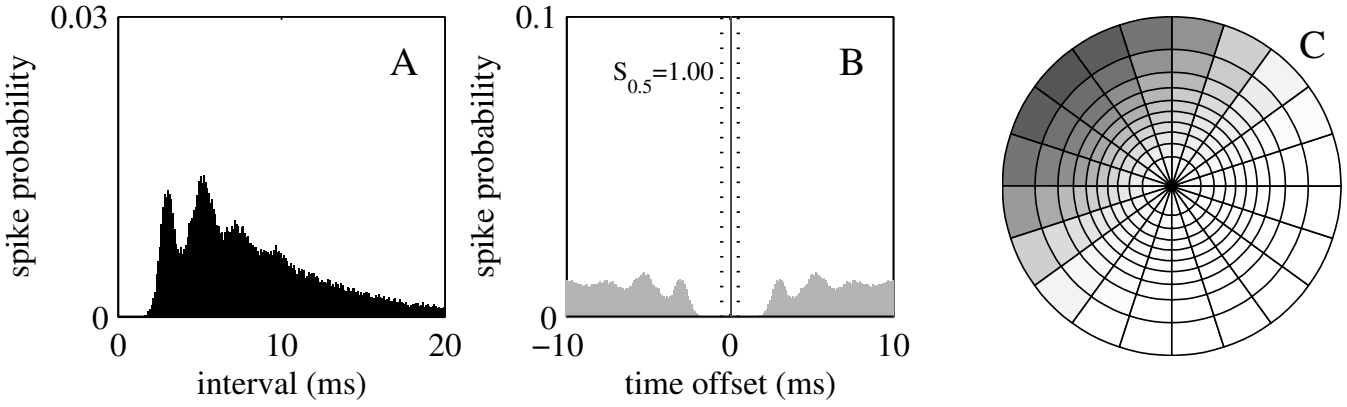

Figure 3: Zurvan as a model of Zurvan. (A) ISI histogram for the model, (B) cross-correlogram (light grey) with ITI overlaid (dark grey), dotted lines indicate limits of similarity metric $S_{\Delta t}$, (C) response probability profile of model, showing strongest response to velocity vectors around $3\pi/4$.

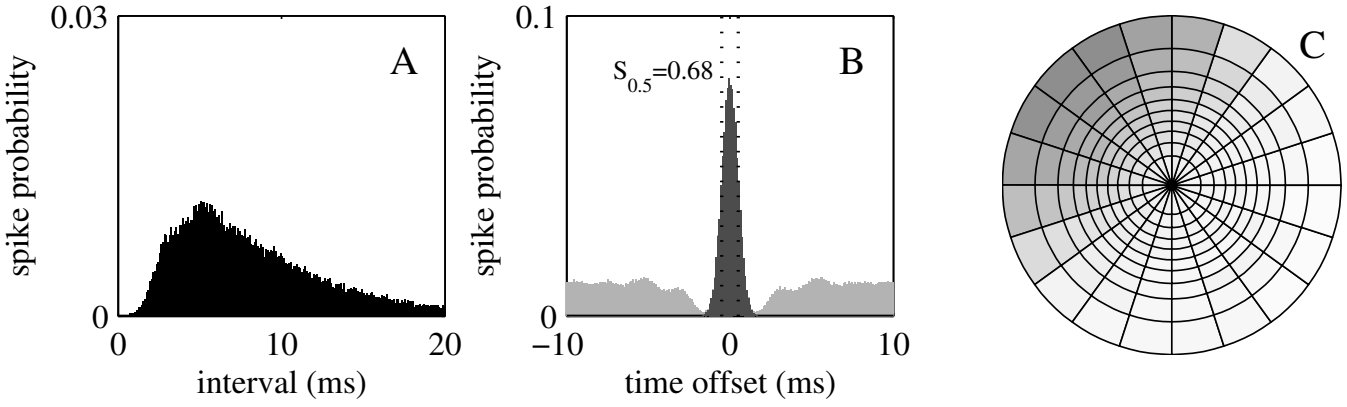

Figure 4: Noisy Zurvan as a model of Zurvan, sub-panels as for Figure 3.

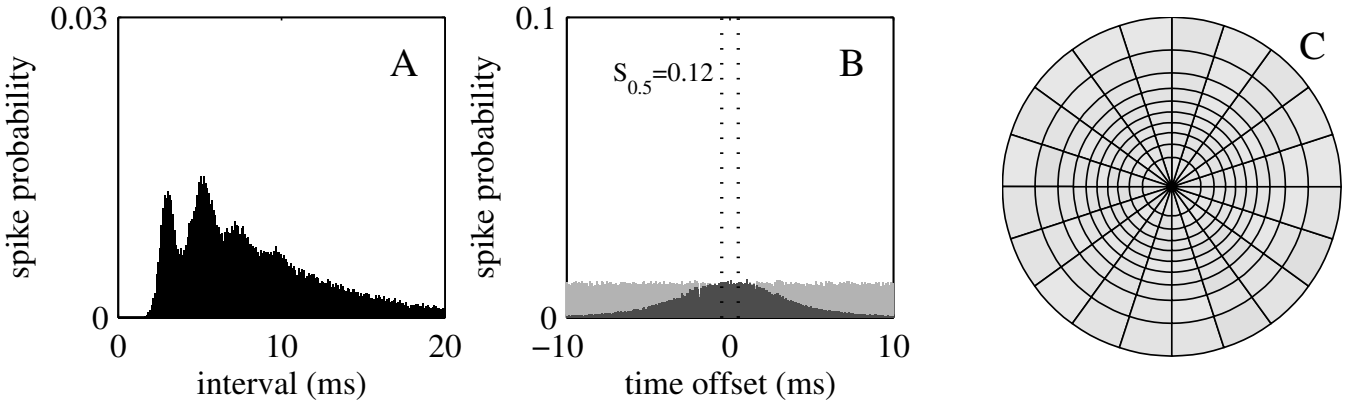

Figure 5: Time-shifted Zurvan as a model of Zurvan, sub-panels as for Figure 3.

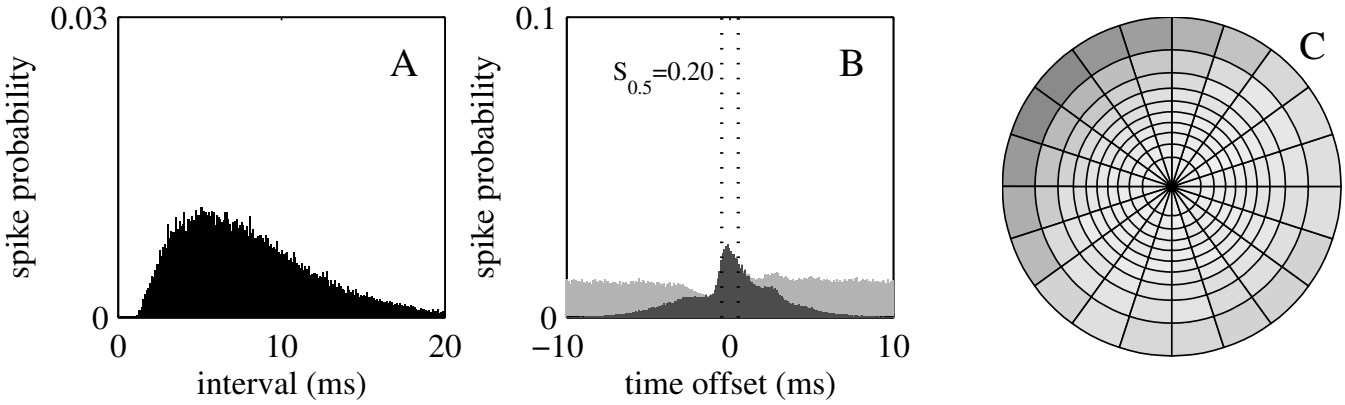

Figure 6: Z1 as a model of Zurvan, sub-panels as for Figure 3.

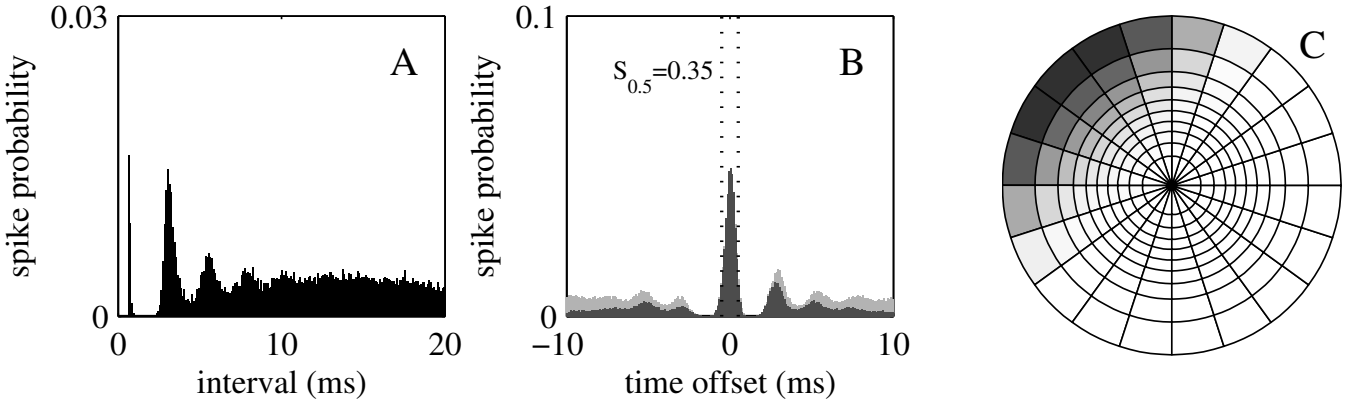

Figure 7: Z2 as a model of Zurvan, sub-panels as for Figure 3.

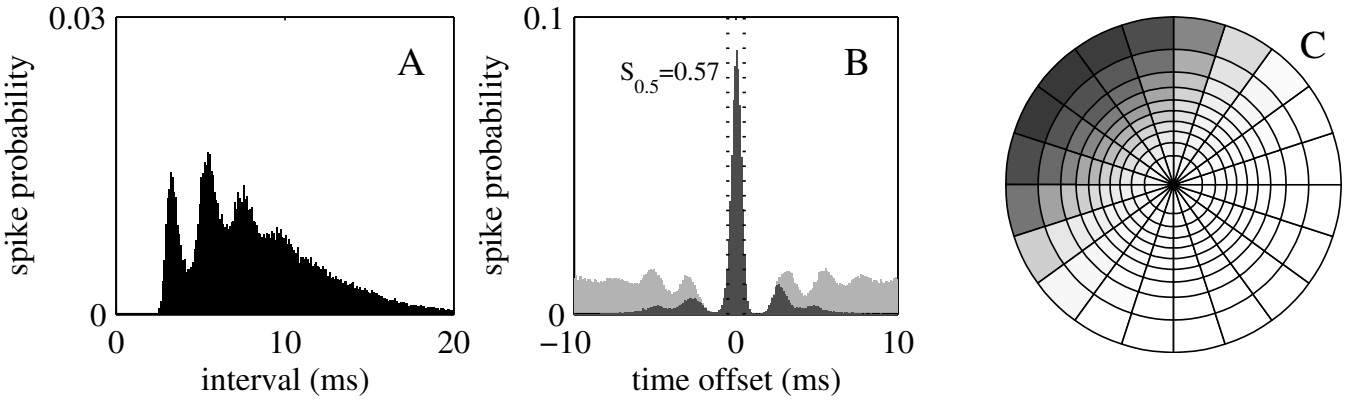

Figure 8: Z4 as a model of Zurvan, sub-panels as for Figure 3.

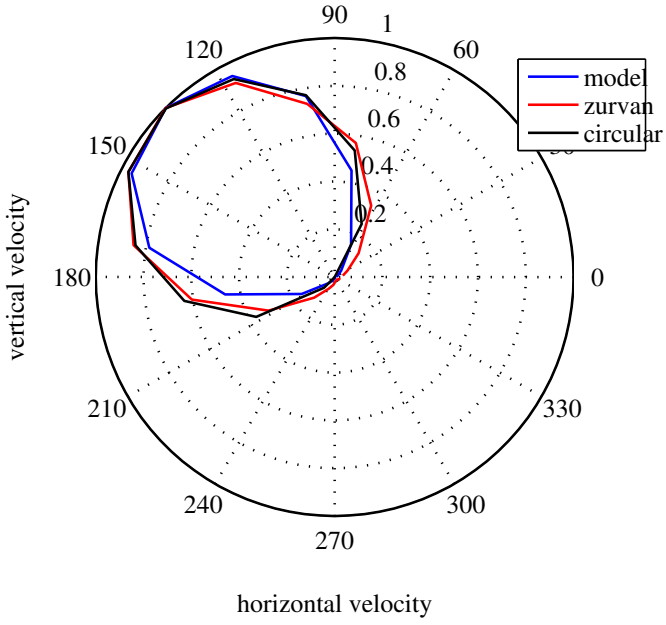

Figure 9: Angular response profiles computed from response probability profiles for Zurvan and Z4, compared with true circle.

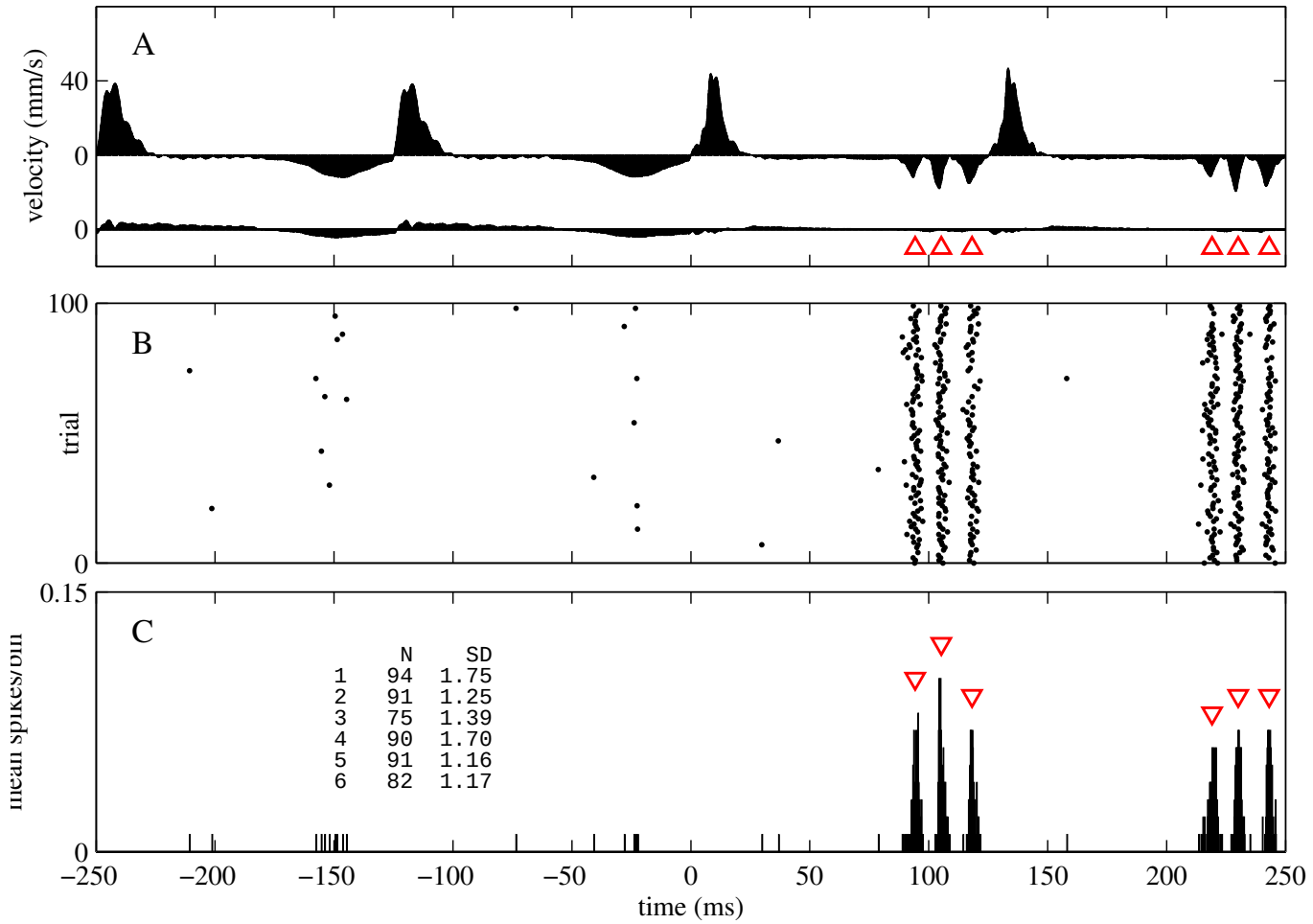

Figure 10: Response of Z4 to the natural data for P280 texture, 100 different stimuli. (A) Average stimulus velocity profile showing two free whisks followed by two whisks against the texture, (B) response raster plot, (C) response PSTH. Arrowheads indicate velocity features to which Zurvan responded (A) and Z4 response peaks (C). Figures in lower panel indicate total spikes (N) over all trials in response to each feature, and standard deviation in spike time of these (SD).

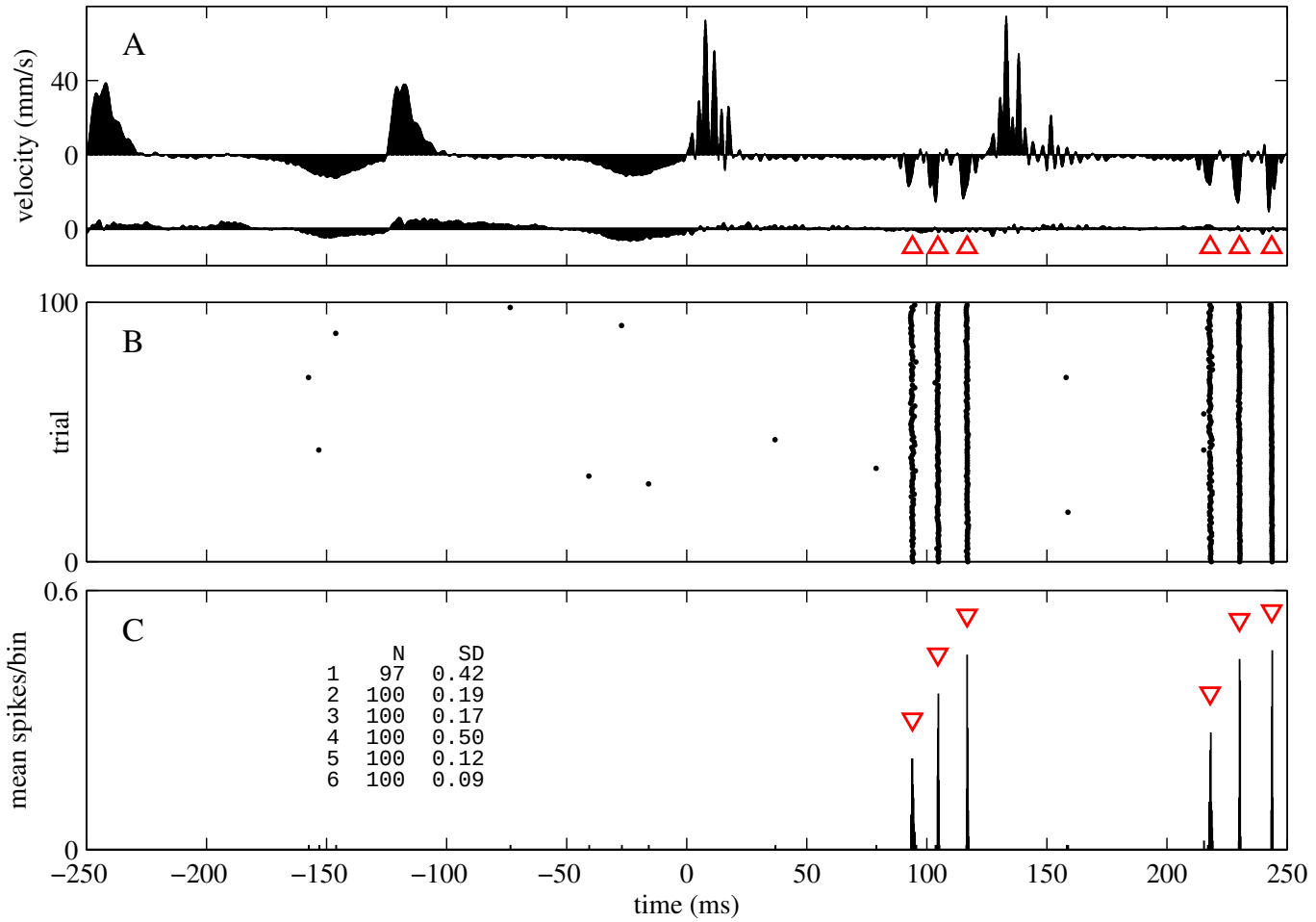

Figure 11: Response of Z4 to the natural data for P280 texture, 100 identical stimuli. See figure above for details, except (A) repeated velocity profile.

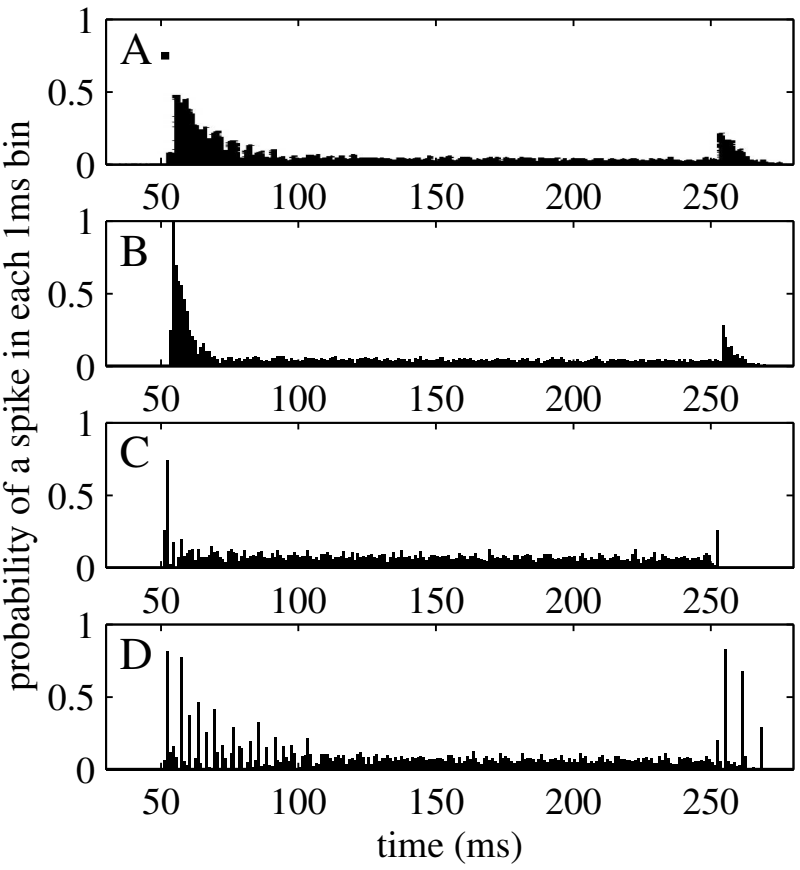

Figure 12: Memory and mechanical ringing. (A) Reproduction of population response histogram for ramp-hold-release stimulus with 3ms rise time, from Shoykhet *et al.*, 2000, top left panel of Figure 1 in that work – short floating bar at 50ms indicates duration of 3ms stimulus ramp. Simulation of that protocol driving model cells produces results: (B) original follicle model, (C) original follicle model with memory component removed, and (D) as (C) but with actuator ringing modelled by stimulus filtering (see text for details).